Injectable Nanocomposites of Single-Walled Carbon Nanotubes and Biodegradable Polymers for Bone Tissue Engineering

Xinfeng Shi,[†] Jared L. Hudson,[‡] Patrick P. Spicer,[†] James M. Tour,[‡] Ramanan Krishnamoorti,[§] and Antonios G. Mikos*,[†]

Department of Bioengineering, Rice University, MS-142, Houston, Texas 77251-1892, Departments of Chemistry and Mechanical Engineering and Materials Science, and Center for Nanoscale Science and Technology, Rice University, MS-222, Houston, Texas 77251-1892, and Department of Chemical Engineering, University of Houston, Houston, Texas 77204-4004

Received April 21, 2006; Revised Manuscript Received May 16, 2006

We have investigated the dispersion of single-walled carbon nanotubes (SWNTs) and functionalized SWNTs (F-SWNTs) in the unsaturated, biodegradable polymer poly(propylene fumarate) (PPF) and examined the rheological properties of un-cross-linked nanocomposite formulations as well as the electrical and mechanical properties of cross-linked nanocomposites. F-SWNTs were produced from individual SWNTs by a diazonium-based method and dispersed better than unmodified SWNTs in both un-cross-linked and cross-linked PPF matrix. Cross-linked nanocomposites with F-SWNTs were superior to those with unmodified SWNTs in terms of their mechanical properties. Specifically, nanocomposites with 0.1 wt % F-SWNTs loading resulted in a 3-fold increase in both compressive modulus and flexural modulus and a 2-fold increase in both compressive offset yield strength and flexural strength when compared to pure PPF networks, whereas the use of 0.1 wt % SWNTs gained less than 37% mechanical reinforcement. These extraordinary mechanical enhancements considered together with Raman scattering and sol fraction measurements indicate strong SWNT−PPF interactions and increased cross-linking densities resulting in effective load transfer. With enhanced mechanical properties and capabilities of in situ injection and cross-linking, these SWNT/polymer nanocomposites hold significant implications for the fabrication of bone tissue engineering scaffolds.

Introduction

Synthetic biodegradable polymers are widely utilized in the fabrication of scaffolds for bone tissue engineering.[1,2] However, this class of materials generally exhibits inferior mechanical properties when used in scaffolds of high porosity for guided bone growth under load bearing conditions.[2,3] In this study, single-walled carbon nanotubes (SWNTs) were applied as reinforcing agents based on their extremely high mechanical properties and aspect ratio.[4−6] Poly(propylene fumarate) (PPF), an injectable, cross-linkable, and biodegradable polymer,[7] was chosen as the polymer matrix since this polymer has been utilized to form highly porous scaffolds for load-bearing bone repair.[8]

A major challenge for mechanical reinforcement via SWNTs is to overcome strong inter-tube aggregation, resulting from van der Waals interactions and $\pi-\pi$ stacking, to prevent the formation of large bundles of SWNTs.[9] Such bundles or aggregates may cause slippage between nanotubes, become stress concentrators, or initiate cracks under applied loads.[5,10] We have previously shown that SWNTs can be dispersed reasonably well in PPF with the observation of van Hove singularities in the absorption spectra and geometrical percolation at SWNT loadings of ~0.03 wt %.[11] Those results suggested an inherent attraction between the SWNTs and PPF, presumably originating from Lewis acid/Lewis base interactions, and therefore indicated the strong potential of SWNTs for mechanical reinforcement of the cross-linked PPF.

Here, we modified the side walls of individual SWNTs by a diazonium-based functionalization mechanism[12] to further improve nanotube dispersion through steric stabilization. The effects of incorporating these functionalized SWNTs (F-SWNTs) into PPF polymer and the interactions between nanotubes and matrix were examined. The questions addressed by this study are as follows: (1) Can covalent functionalization improve SWNT dispersion in PPF before and after cross-linking? (2) Can F-SWNTs further enhance the mechanical properties of cross-linked nanocomposites compared to unfunctionalized SWNTs? (3) What are the mechanisms for the mechanical reinforcement of these nanocomposites?

Materials and Methods

Polymer Synthesis. Poly(propylene fumarate) (PPF) and its cross-linking agent poly(propylene fumarate)-diacrylate (PPF-DA) were synthesized as previously described.[13,14] Both polymer structures were confirmed by ^{1}H NMR. The PPF used in this study had a number average molecular weight (M_n) of 1600 and a polydispersity index of 2.2, measured by gel permeation chromatography (GPC) with a differential refractive index detector (Waters, Milford, MA) using a Styragel HR 4E 7.8 × 300 mm column (Waters, Milford, MA). A calibration curve generated from polystyrene standards (Fluka, Switzerland) with peak molecular weights ranging from 374 to 28 000 was used to determine PPF molecular weights. PPF-DA has one fumarate unit surrounded by two terminal acrylate groups and has a molecular weight of 340. All reagents and organic solvents were used as received.

* Corresponding author. Phone: (713) 348-5355. Fax: (713) 348-4244. E-mail: mikos@rice.edu.

[†] Department of Bioengineering, Rice University.

[‡] Departments of Chemistry and Mechanical Engineering and Materials Science, and Center for Nanoscale Science and Technology, Rice University.

[§] University of Houston.

10.1021/bm060391v CCC: $33.50
Published on Web 06/16/2006

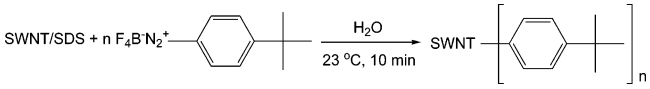

Figure 1. Schematic of the functionalization of individual SWNTs wrapped with sodium dodecyl sulfate (SDS) surfactant.

SWNT Functionalization and Characterization. The SWNTs used for this study were produced by a high pressure carbon monoxide (HiPco) process and purified as previously described.[15,16] The purified SWNTs were then functionalized by a diazonium-based method (Figure 1).[12] Briefly, 4-*tert*-butylbenzenediazonium tetrafluoroborate (1.64 g, 6.6 mmol) was added to 1 L of a sodium dodecyl sulfate (SDS) suspension of SWNTs (40 mg, 3.3 mmol of carbon). The pH of the solution was adjusted to pH 10 with 6 M NaOH, and the mixture was subsequently allowed to stir for 3 h. The mixture was then diluted with acetone and filtered through a 1 μm polycarbonate membrane filter. The filter cake was washed with water (300 mL) and acetone (300 mL) and then dried to give functionalized SWNTs (50 mg). The mass loss in thermogravimetric analysis (TGA, 10 °C/min to 750 °C in argon) was 29%, which indicated that one out of every 27 carbon atoms on the walls of SWNTs was covalently attached with a 4-*tert*-butylphenylene group.

Nanocomposite Preparation. SWNTs were first dispersed in chloroform by high shear mixing for 5 min and sonication (700 W ULTRAsonik 28× bath cleaner, Ney Dental, Yucaipa, CA) for 15 min and were immediately added to a chloroform solution of PPF and the cross-linking agent PPF-DA (consisting of 1 g PPF and 2 g PPF-diacrylate per 3 mL chloroform) to prevent any settling. After further sonication for 15 min, the chloroform was removed by rotary evaporation and vacuum-drying.

Melt-State Rheology. The melt-state rheology measurements of uncross-linked nanocomposites were performed with an AR1000 rheometer (TA Instruments, New Castle, DE) in a linear dynamic oscillatory shear mode using 0.01−0.1 strain amplitude at 25 °C. Each melt sample was placed between a base plate and a cone geometry (60 mm diameter, 59 min cone angle, and 26 μm truncation), and the complex viscosity magnitude ($|\eta^*|$), storage modulus (G'), and loss modulus (G'') were recorded as a function of the oscillatory strain frequency (ω) of 0.001−30 Hz. The complex shear modulus magnitude ($|G^*|$) is defined as follows:

$$|G^*| = (G'^2 + G''^2)^{1/2}$$

Thermal Polymerization and Specimen Fabrication. Thermal polymerization of nanocomposites was triggered by the addition of 1 wt % benzoyl peroxide (BP, free-radical initiator) and 0.15 wt % *N*,*N*-dimethyl-*p*-toluidine (DMT, accelerator). BP was dissolved in diethyl fumarate at a concentration of 0.1 g/mL and administered into the mixture followed by the addition of DMT under vigorous stirring to initiate the thermal cross-linking reaction.

To fabricate specimens for electrical conductivity testing, the polymeric mixture was poured on a glass plate and then compressed into a thin film by another glass plate with a 0.7 mm gap between the two plates. After curing at 37 °C for 24 h, the film was cut by a blade into specimens of 2 cm width and 6 cm length. To make specimens for mechanical testing, the mixture was filled into cylindrical glass vials of 6.5 mm diameter and 40 mm length for compressive testing or injected into cylindrical glass tubes of 3 mm diameter and 150 mm length for flexural testing. Both types of specimens were centrifuged at 721*g* for 5 min to remove any air bubbles and then cured at 37 °C for 24 h. The specimens were recovered by breaking the glass container and then cut to the proper lengths with a diamond saw (South Bay Technology Model 650, San Clemente, CA). For compressive testing specimens, the length was twice their diameter (approximately 6.5 mm diameter and 13 mm length) and the two ends were flat and perpendicular to their long axis. The flexural testing specimens had dimensions of roughly 3 mm diameter and 60 mm length.

Electrical Conductivity. Electrical conductivities of cross-linked nanocomposites were measured at room temperature using a four-point probe method with a Keithley model 2400 Series SourceMeter (Keithley Instruments, Cleveland, OH). The percolation threshold p_c was calculated using the scaling law[17]

$$\sigma = m\,(p - p_c)^t$$

where σ is the electrical conductivity, p is the concentration of SWNTs, t is a universal scaling exponent, and m is a constant.

Electron Microscopy. Thin sections (50−100 nm in thickness) of the cross-linked nanocomposites were prepared using a Leica Ultracut microtome (Leica, Vienna, Austria) and then examined with a JEOL 2010 transmission electron microscope (TEM; JEOL U.S.A., Peabody, MA). The fracture surfaces of tested specimen from mechanical testing were sputter-coated with gold and then examined with a JEOL 6500F scanning electron microscope (SEM; JEOL U.S.A.) at an accelerating voltage of 15 kV.

Mechanical Testing. Two types of mechanical testing, compression and flexion, were conducted with cross-linked specimens at room temperature using an 858 Material Testing System mechanical testing machine (MTS System Corporation, Eden Prairie, MN) with five specimens tested for each sample group ($n = 5$).

Compressive testing was carried out in accordance with the American Society of Testing Materials (ASTM) Standard D695-02a. The prepared cylindrical specimens were compressed along their long axis until failure. The force and displacement were recorded throughout the compression and converted to stress and strain based on the initial specimen dimensions. The compressive modulus was calculated as the slope of the initial linear portion of the stress−strain curve. The offset compressive yield strength was determined as the stress at which the stress−strain curve intersected with a line drawn parallel to the slope defining the modulus, beginning at 1.0% strain (offset).

Flexural testing was performed in accordance with ASTM Standard D790-03. The testing specimens were placed on a three-point bending apparatus with two supports spanning 40 mm from each other and loaded by means of a loading nose midway between the supports until failure. In a manner similar to that of compressive testing, the recorded force and displacement were converted to a stress−strain curve and the flexural modulus was calculated from the stress−strain curve. The flexural strength was defined as the maximum stress carried by the specimen during the flexural testing.

Raman Spectroscopy. The Raman spectra of SWNTs and their uncross-linked and cross-linked nanocomposites were collected by a Renishaw 1000 MicroRaman System (Renishaw plc, New Mills, United Kindom) with a 514.5 nm Ar-ion laser. The polarized Raman spectroscopy was used to assess the alignment of SWNTs in the cross-linked specimens. The specimen on a rotational stage was rotated at various angles with respect to the polarized excitation, and the signal intensities were recorded using the same Raman system with a vertical−vertical (VV) configuration excited by a 632.8 nm HeNe laser. Both measurements were repeated over three different spots on each sample surface.

Sol Fraction. Sol fraction was measured by assessment of the fraction of cross-linked polymer/nanocomposite solubilized by methylene chloride. Sol fraction was measured on the basis that un-cross-linked PPF, PPF-DA, and their oligomers are soluble in methylene chloride while the cross-linked polymer network is not. In a typical experiment, a sample of approximately 0.5 g was weighed (W_i, accurate to 0.001 g) and placed into a vial with 20 mL of methylene chloride. The vial was sealed and placed on a shaker table (80 rpm) at room temperature for 7 days. The solid sample was then collected by filtration with weighed filter paper (W_p). The filter paper with retained material was dried at 60 °C for 1 h and at room temperature for another 1 h and then weighed again (W_{p+s}). The sol fraction was calculated by the following equation and the testing was repeated five times for each sample group ($n = 5$).

$$\text{sol fraction} = \frac{W_i - (W_{p+s} - W_p)}{W_i} \times 100\%$$

Statistical Analysis. All statistical comparisons were conducted with a 95% confidence interval ($p < 0.05$). Single-factor analysis of variance (ANOVA) was conducted to identify significant differences among treatment groups. When significant differences were present, Tukey's Honestly Significantly Different (HSD) multiple-comparison test was used to determine the potential effects. The data from mechanical testing and sol fraction measurements were expressed as means ± standard deviation for $n = 5$ for each sample group.

Results and Discussion

SWNT Functionalization. It has been previously shown that surfactants (anionic, cationic, or nonionic) can disperse SWNTs in water at concentrations well below the critical micelle surfactant concentration.[18] In the present work, individual nanotubes were stabilized in an aqueous solution by the addition of sodium dodecyl sulfate (SDS)[19] and then covalently attached with a 4-*tert*-butylphenylene group (using 4-*tert*-butylbenzenediazonium tetrafluoroborate) which prevents the rebundling of the nanotubes presumably by a steric stabilization mechanism (Figure 1).[9] This functional group may also provide possible covalent linkages between the SWNTs and the PPF network upon curing of the polymer.[20]

SWNT Dispersion and Melt-State Rheology. A well-dispersed carbon nanotube/polymer system is usually characterized by a geometrically percolated nanotube network that exhibits solidlike character.[21−24] In this study, SWNTs and functionalized SWNTs (F-SWNTs) could be uniformly dispersed throughout the PPF matrix to form such networks. For un-cross-linked nanocomposites, the formation of these nanotube superstructures was demonstrated by melt-state rheological characteristics (Figure 2). In particular, PPF, a viscous liquid without SWNTs, became solidlike with SWNT loadings in excess of the geometric percolation threshold. As shown in Figure 2 and a previous study,[11] the geometrical percolation was found to occur at nanotube loadings of less than 0.02 and ~0.03 wt % for F-SWNTs and SWNTs, respectively. Clearly, the additional steric stabilization provided by individualized nanotubes combined with perhaps more favorable thermodynamic interactions among F-SWNTs and PPF permits better dispersion of F−SWNTs when compared to SWNT composites. A comparison of the complex viscosity magnitude ($|\eta^*|$, at a fixed frequency) further illustrates this concept. F-SWNT nanocomposites have a significantly higher viscosity than the corresponding (i.e., identical nanotube loading) SWNT nanocomposites (Figure 2).

SWNT Dispersion and Electrical Conductivity. These SWNT and F-SWNT based PPF nanocomposites can be poured or injected into molds with various shapes and then cross-linked by a thermal polymerization method.[11] We conjecture that the dispersion state of SWNTs in PPF was largely unchanged by the cross-linking reaction as the electrical percolation threshold for the cross-linked SWNT nanocomposites was found to be ~0.03 wt % (Figure 3), similar to the geometrical percolation threshold for un-cross-linked nanocomposites. The solid-state electrical conductivity of cross-linked F-SWNT nanocomposites did not increase with higher loading of F-SWNTs. This is because the covalent functionalization disrupts the electronic structure of nanotubes and makes them insulating.[25]

Electron Microscopy. Transmission electron microscopy (TEM) and scanning electron microscopy (SEM) were used to further confirm that F-SWNTs remained well dispersed in the cross-linked PPF matrix. As shown in Figure 4A, SWNTs tended to form micron-size aggregates at 0.1 wt % loadings. On the contrary, F-SWNTs existed as individual tubes or small bundles of only 2−3 individual nanotubes throughout the polymer matrix (Figure 4B). This nearly individual dispersion persisted in all F-SWNT nanocomposites, including those with nanotube loadings higher than 0.1 wt %. More interestingly, the broken/protruded F-SWNTs seen along the fracture surfaces of nanocomposites were covered by a layer of polymer, suggesting strong interactions between nanotubes and polymer even after cross-linking.

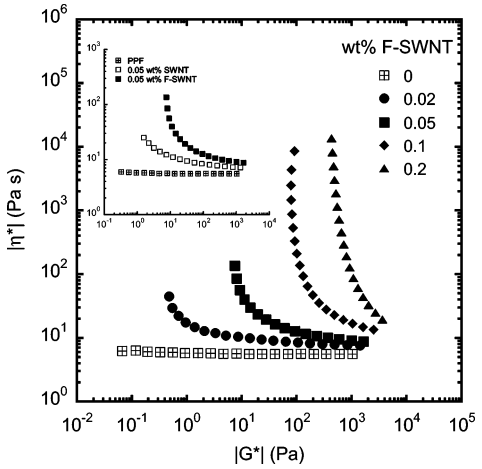

Figure 2. Complex viscosity magnitude ($|\eta^*|$) vs complex shear modulus magnitude ($|G^*|$) for un-cross-linked nanocomposite formulations at various F-SWNT concentrations. The inset includes the corresponding values for the 0.05 wt % SWNT formulation for comparison purposes.

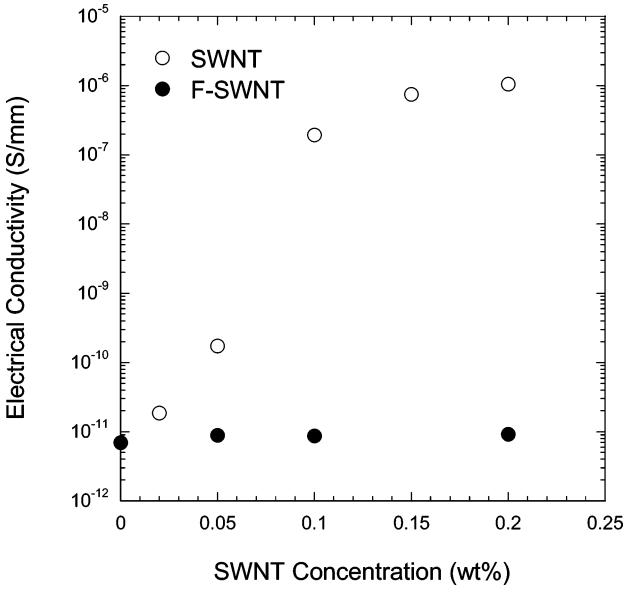

Figure 3. Electrical conductivity as a function of nanotube concentration for SWNT and F-SWNT cross-linked nanocomposites. A value of 0.03 wt % is estimated for the electrical percolation threshold of SWNT nanocomposites using the scaling law.

Mechanical Properties. Extraordinary mechanical reinforcements were achieved with F−SWNT/PPF nanocomposites (Table 1). In particular, the mechanical reinforcement provided by F-SWNTs exceeded the enhancements observed with the SWNTs, indicating the importance of better dispersion and possible mechanical coupling between the functionalized nanotubes and the PPF matrix. For the F-SWNT nanocomposites,

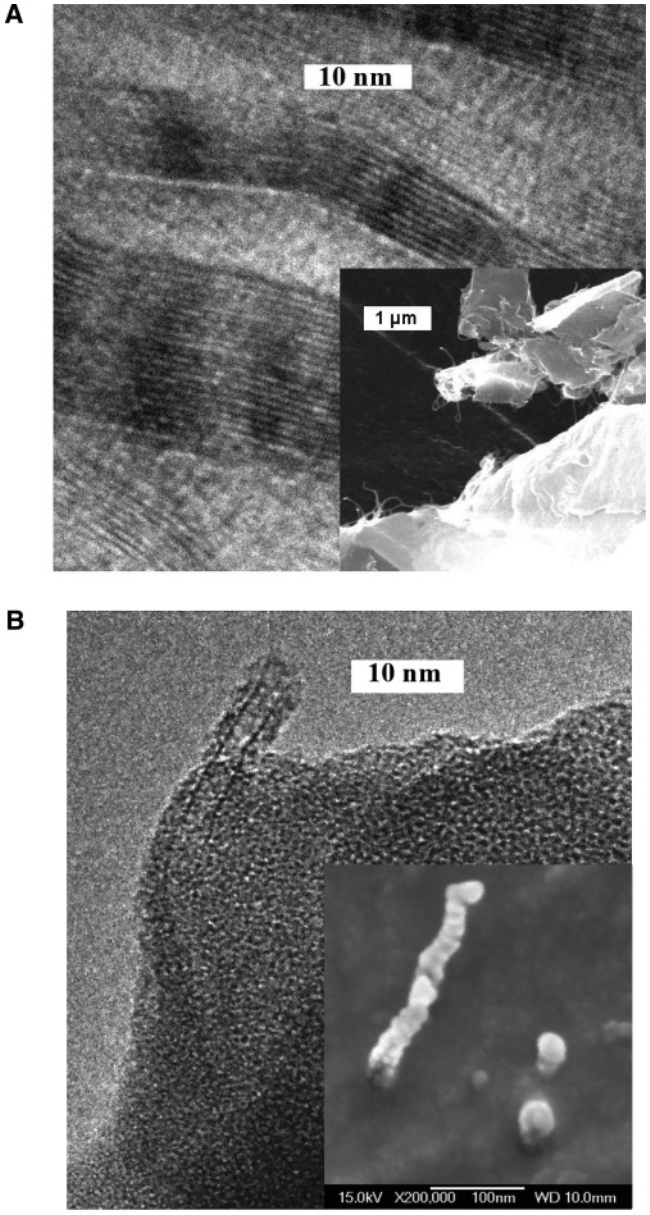

Figure 4. (A) TEM image of a section of cross-linked 0.1 wt % SWNT nanocomposite with large nanotube bundles embedded in PPF. The lower right inset is a SEM image of the fracture surface of the same sample after flexural mechanical testing. Micron-size aggregates of SWNTs (bright color) were seen on the polymer (dark background). The scale bar corresponds to 10 nm in the TEM image and 1 μm in the SEM image. (B) TEM image of a section of cross-linked 0.1 wt % F-SWNT nanocomposite. A small bundle of a few individual nanotubes covered by a layer of PPF was drawn out of the edge of the nanocomposite section. The lower right inset shows a SEM image of the fracture surface of the same sample after flexural mechanical testing. F-SWNTs covered by a layer of PPF were observed along the fracture surface. The scale bar corresponds to 10 nm in the TEM image and 100 nm in the SEM image.

mechanical properties were significantly enhanced with increasing nanotube loadings. With merely 0.1 wt % F-SWNT loading, a roughly 3-fold increase in both compressive modulus and flexural modulus and a greater than 2-fold increase in both compressive offset yield strength and flexural strength were observed when compared to pure PPF networks. Beyond 0.1 wt % F-SWNT loading, mechanical properties of these nanocomposites began to decline with the observation of large deviations between repeat measurements. It should be noted that this decline may be due to the presence of air bubbles retained during specimen fabrication since the high viscosities of these nanocomposites impairs proper processing.

Table 1. Experimental Values of Mechanical Properties of Crosslinked PPF as Well as SWNT and F-SWNT Nanocomposites for Nanotube Concentrations Ranging from 0.01 to 0.2 wt % (Mean $\pm$ Standard Deviation for $n = 5$)

	compressive mechanical property		flexural mechanical property	
	compressive modulus (MPa)	offset yield strength (MPa)	flexural modulus (MPa)	flexural strength (MPa)
PPF polymer	318 $\pm$ 34	11.8 $\pm$ 3.5	456 $\pm$ 25	28.4 $\pm$ 1.4
SWNT Nanocomposites				
0.01 wt %	450 $\pm$ 25	19.0 $\pm$ 0.6	450 $\pm$ 59	25.1 $\pm$ 2.1
0.02 wt %	527 $\pm$ 59	19.1 $\pm$ 2.3	425 $\pm$ 92	29.2 $\pm$ 4.9
0.05 wt %	468 $\pm$ 29	15.8 $\pm$ 2.1	551 $\pm$ 63	33.9 $\pm$ 3.5
0.10 wt %	391 $\pm$ 40	14.7 $\pm$ 1.5	623 $\pm$ 62	36.3 $\pm$ 2.4
0.20 wt %	416 $\pm$ 51	12.2 $\pm$ 3.5	578 $\pm$ 167	34.2 $\pm$ 7.6
F-SWNT Nanocomposites				
0.01 wt %	432 $\pm$ 55	15.7 $\pm$ 1.6	600 $\pm$ 45	40.5 $\pm$ 0.9
0.02 wt %	542 $\pm$ 14	21.1 $\pm$ 0.5	726 $\pm$ 80	40.3 $\pm$ 5.0
0.05 wt %	680 $\pm$ 48	25.0 $\pm$ 2.9	765 $\pm$ 26	43.5 $\pm$ 1.5
0.10 wt %	981 $\pm$ 108	25.3 $\pm$ 1.9	1335 $\pm$ 173	63.7 $\pm$ 3.6
0.20 wt %	731 $\pm$ 649	22.7 $\pm$ 19.3	1229 $\pm$ 113	38.9 $\pm$ 13.6

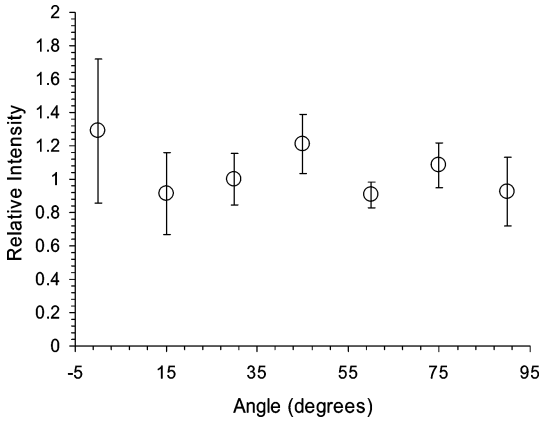

Figure 5. Analysis of polarized Raman spectra of cross-linked 0.1 wt % F-SWNT nanocomposite in the VV configuration excited by a 632.8 nm HeNe laser. Symbols indicate Raman G band relative intensity, averaged with standard deviation over three spots on the sample surface. There is no significant difference among the Raman intensities of the specimen at different rotational angles.

Mechanisms of Mechanical Reinforcement. Possible causes for these dramatic mechanical enhancements include (a) nanotube alignment in the polymer matrix in the direction of centrifugation during the specimen fabrication; (b) alteration of polymer matrix mechanical properties due to the strong interactions between the nanotubes and PPF; (c) higher surface-to-volume ratio provided by the well-dispersed F-SWNTs in the polymer; and/or (d) interaction of percolated F-SWNTs with PPF during cross-linking resulting in a higher density of cross-links and effective load transfer. However, polarized Raman scattering, an accepted tool for assessing the alignment of SWNT structures,[26−28] indicates that virtually no alignment exists among nanotubes in the cross-linked nanocomposites (Figure 5). Clearly, although not negligible as illustrated from a previous study of the SWNT-based PPF nanocomposites,[11] the interactions between the nanotubes and the polymer and their

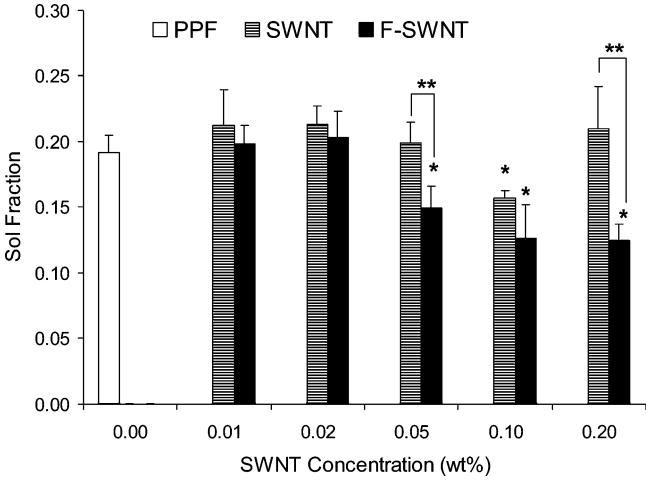

Figure 6. Sol fraction of the cross-linked nanocomposites with various loading of SWNTs and F-SWNTs. Error bars represent mean ± standard deviation for $n = 5$. The symbol * indicates a statistically significant difference between the indicated nanocomposite and pure polymer and the symbol ** indicates a statistically significant difference between two SWNT nanocomposites ($p < 0.05$).

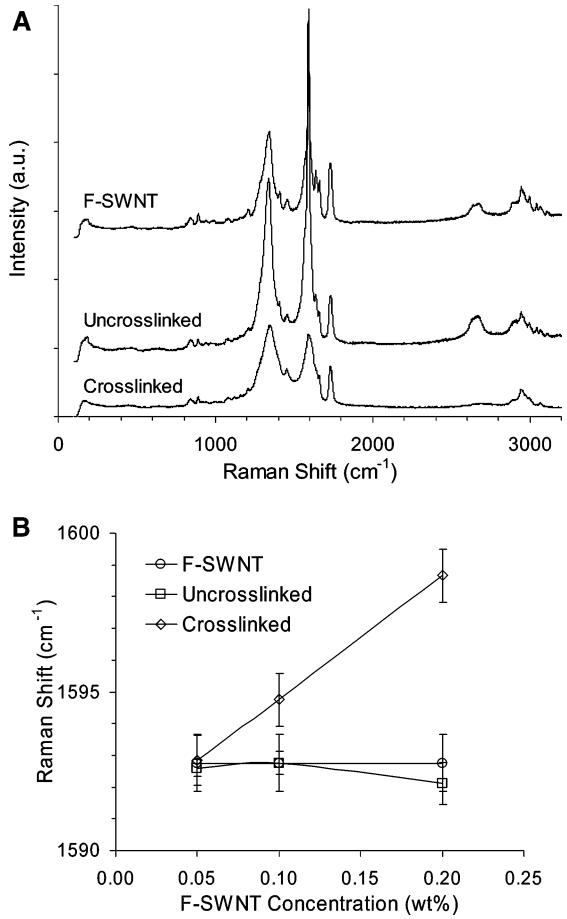

Figure 7. Raman spectroscopy of specimens excited by a 514.5 nm argon laser. (A) Raman spectra of F-SWNT, un-cross-linked and cross-linked 0.2 wt % F-SWNT nanocomposites. (B) Raman shifts of the tangential (G) bands of F-SWNT, un-cross-linked and cross-linked F-SWNT nanocomposites as a function of the F-SWNT concentration. Symbols indicate Raman G band peak positions, averaged with standard deviation over three spots on the sample surface.

consequences on the mechanical properties of the matrix are insufficient to explain the large reinforcements observed for the F-SWNT nanocomposites. On the other hand, analysis of the sol fraction of composites (Figure 6) indicates a higher cross-linking density for the F-SWNT nanocomposites than the PPF networks, suggesting the possibility of nanotube−PPF cross-links. Furthermore, Raman scattering data of the tangential mode (G-mode) of nanotubes in the cross-linked nanocomposites indicates significant upshift with increased F-SWNT loading (Figure 7, panels A and B). Specifically, 0.2 wt % F-SWNT nanocomposite exhibited a 6 cm^{-1} upshift. This shift is generally believed to be caused by the residual strain and load transfer to the nanotubes from the polymer matrix,[29,30] which is enhanced for well-dispersed F-SWNTs because of the increased interfacial area and cross-linking density.

Conclusions

Our goal in this study was to investigate the effects of functionalization of SWNTs on their dispersion in PPF polymer and the mechanical reinforcement of cross-linked nanocomposites. Compared to unfunctionalized SWNTs, F-SWNTs were better dispersed as nearly individual nanotubes throughout the PPF matrix to form percolated networks at 0.02 wt % and higher loadings. For the first time, significant mechanical reinforcement, a 3-fold increase in both compressive modulus and flexural modulus and 2-fold increase in both compressive offset yield strength and flexural strength of polymer networks, has been achieved with a mere 0.1 wt % loading of F−SWNTs. The formation SWNT-PPF cross-links and subsequent effective load transfer may explain these extraordinary mechanical enhancements. As demonstrated here, these SWNT/polymer nanocomposites are fabricated through a process suitable for in situ injection and cross-linking, and their mechanical properties can be modulated through alteration of nanotube loading, making them promising materials for tissue engineering applications.

Acknowledgment. This research was supported by grants from the National Institutes of Health (R01 AR42639), the Nanoscale Science and Engineering Initiative of the National Science Foundation (EEC-0118001), the National Science Foundation (DMR 9875321), and the Robert A. Welch Foundation. The work of J.M.T. was sponsored by AFOSR, NASA, and ONR. R.K. acknowledges the hospitality of the Department of Bioengineering at Rice University during his sabbatical. Support of the Texas Institute for Intelligent Bio-Nano Materials and Structures for Aerospace Vehicles, funded by NASA Cooperative Agreement No. NCC-1-02038, is gratefully acknowledged by R.K. We thank Dr. Wenhua Guo for assistance with the transmission electron microscopy.

References and Notes

(1) Langer, R.; Vacanti, J. P. *Science* **1993**, *260*, 920−926.
(2) Mistry, A. S.; Mikos, A. G. *Adv. Biochem. Eng. Biotechnol.* **2005**, *94*, 1−22.
(3) Schaefer, D.; Martin, I.; Jundt, G.; Seidel, J.; Heberer, M.; Grodzinsky, A.; Bergin, I.; Vunjak-Novakovic, G.; Freed, L. E. *Arthritis Rheum.* **2002**, *46*, 2524−2534.
(4) Calvert, P. *Nature* **1999**, *399*, 210−211.
(5) Ajayan, P. M.; Schadler, L. S.; Giannaris, C.; Rubio, A. *Adv. Mater.* **2000**, *12*, 750−753.
(6) Zhang, X. F.; Liu, T.; Sreekumar, T. V.; Kumar, S.; Moore, V. C.; Hauge, R. H.; Smalley, R. E. *Nano Lett.* **2003**, *3*, 1285−1288.
(7) Shi, X.; Mikos, A. G. Poly(propylene fumarate). In *An Introduction to Biomaterials*; Guelcher, S. A., Hollinger, J. O., Eds.; CRC Press: Boca Raton, FL, 2006; pp 205−218.
(8) Hedberg, E. L.; Shih, C. K.; Lemoine, J. J.; Timmer, M. D.; Liebschner, M. A. K.; Jansen, J. A.; Mikos, A. G. *Biomaterials* **2005**, *26*, 3215−3225.

(9) Dyke, C. A.; Tour, J. M. *Chem.—Eur. J.* **2004**, *10*, 813−817.
(10) Ajayan, P. M.; Banhart, F. *Nat. Mater.* **2004**, *3*, 135−136.
(11) Shi, X.; Hudson, J. L.; Spicer, P. P.; Tour, J. M.; Krishnamoorti, R.; Mikos, A. G. *Nanotechnology* **2005**, *16*, S531−S538.
(12) Dyke, C. A.; Tour, J. M. *Nano Lett.* **2003**, *3*, 1215−1218.
(13) Timmer, M. D.; Ambrose, C. G.; Mikos, A. G. *J. Biomed. Mater. Res.* **2003**, *66A*, 811−818.
(14) Shung, A. K.; Timmer, M. D.; Jo, S.; Engel, P. S.; Mikos, A. G. *J. Biomater. Sci. Polym. Ed.* **2002**, *13*, 95−108.
(15) Chiang, I. W.; Brinson, B. E.; Huang, A. Y.; Willis, P. A.; Bronikowski, M. J.; Margrave, J. L.; Smalley, R. E.; Hauge, R. H. *J. Phys. Chem. B* **2001**, *105*, 8297−8301.
(16) Nikolaev, P.; Bronikowski, M. J.; Bradley, R. K.; Rohmund, F.; Colbert, D. T.; Smith, K. A.; Smalley, R. E. *Chem. Phys. Lett.* **1999**, *313*, 91−97.
(17) Chatterjee, T.; Yurekli, K.; Hadjiev, V. G.; Krishnamoorti, R. *Adv. Funct. Mater.* **2005**, *15*, 1832−1838.
(18) Matarredona, O.; Rhoads, H.; Li, Z.; Harwell, J. H.; Balzano, L.; Resasco, D. E. *J. Phys. Chem. B* **2003**, *107*, 13357−13367.
(19) O'Connell, M. J.; Bachilo, S. M.; Huffman, C. B.; Moore, V. C.; Strano, M. S.; Haroz, E. H.; Rialon, K. L.; Boul, P. J.; Noon, W. H.; Kittrell, C.; Ma, J. P.; Hauge, R. H.; Weisman, R. B.; Smalley, R. E. *Science* **2002**, *297*, 593−596.
(20) Zhu, J.; Peng, H. Q.; Rodriguez-Macias, F.; Margrave, J. L.; Khabashesku, V. N.; Imam, A. M.; Lozano, K.; Barrera, E. V. *Adv. Funct. Mater.* **2004**, *14*, 643−648.
(21) Mitchell, C. A.; Bahr, J. L.; Arepalli, S.; Tour, J. M.; Krishnamoorti, R. *Macromolecules* **2002**, *35*, 8825−8830.
(22) Kharchenko, S. B.; Douglas, J. F.; Obrzut, J.; Grulke, E. A.; Migler, K. B. *Nat. Mater.* **2004**, *3*, 564−568.
(23) Du, F. M.; Scogna, R. C.; Zhou, W.; Brand, S.; Fischer, J. E.; Winey, K. I. *Macromolecules* **2004**, *37*, 9048−9055.
(24) Hough, L. A.; Islam, M. F.; Janmey, P. A.; Yodh, A. G. *Phys. Rev. Lett.* **2004**, *93*, 168102−1−168102−4.
(25) Bahr, J. L.; Tour, J. M. *J. Mater. Chem.* **2002**, *12*, 1952−1958.
(26) Gommans, H. H.; Alldredge, J. W.; Tashiro, H.; Park, J.; Magnuson, J.; Rinzler, A. G. *J. Appl. Phys.* **2000**, *88*, 2509−2514.
(27) Casavant, M. J.; Walters, D. A.; Schmidt, J. J.; Smalley, R. E. *J. Appl. Phys.* **2003**, *93*, 2153−2156.
(28) Fischer, J. E.; Zhou, W.; Vavro, J.; Llaguno, M. C.; Guthy, C.; Haggenmueller, R.; Casavant, M. J.; Walters, D. E.; Smalley, R. E. *J. Appl. Phys.* **2003**, *93*, 2157−2163.
(29) Hadjiev, V. G.; Mitchell, C. A.; Arepalli, S.; Bahr, J. L.; Tour, J. M.; Krishnamoorti, R. *J. Chem. Phys.* **2005**, *122*, 124708−1−124708−6.
(30) Hadjiev, V. G.; Iliev, M. N.; Arepalli, S.; Nikolaev, P.; Files, B. S. *Appl. Phys. Lett.* **2001**, *78*, 3193−3195.

BM060391V